
Article

Not peer-reviewed version

Surface Ice Velocity near the Terminus of Grey Glacier in the Southern Patagonian Icefield, Based on Direct Field Measurements

[Roberto García-Estebe](#) *

Posted Date: 22 August 2025

doi: [10.20944/preprints202508.1678.v1](https://doi.org/10.20944/preprints202508.1678.v1)

Keywords: glacier surface velocity; ice flow dynamics; glacier retreat; Grey Glacier; Southern Patagonian Icefield



Preprints.org is a free multidisciplinary platform providing preprint service that is dedicated to making early versions of research outputs permanently available and citable. Preprints posted at Preprints.org appear in Web of Science, Crossref, Google Scholar, Scilit, Europe PMC.

Copyright: This open access article is published under a Creative Commons CC BY 4.0 license, which permit the free download, distribution, and reuse, provided that the author and preprint are cited in any reuse.

Disclaimer/Publisher's Note: The statements, opinions, and data contained in all publications are solely those of the individual author(s) and contributor(s) and not of MDPI and/or the editor(s). MDPI and/or the editor(s) disclaim responsibility for any injury to people or property resulting from any ideas, methods, instructions, or products referred to in the content.

Article

Surface Ice Velocity near the Terminus of Grey Glacier in the Southern Patagonian Icefield, Based on Direct Field Measurements

Roberto García-Estebar

Department of Geography, Universidad Nacional de Educación a Distancia, (UNED), Paseo Senda del Rey, 7, 28040 Madrid, Spain; rgarcia@geo.uned.es

Abstract

Climatic variability, topography, and geological-structural controls play a fundamental role in glacier mass balance and ice flow dynamics across multiple temporal scales. Surface ice velocity is a key parameter for understanding these processes. In situ measurements using GPS provide high-precision and high-resolution data, allowing for an objective characterization of glacier dynamics that may be overlooked by remote sensing techniques alone. However, due to the efforts required to collect such direct field data, these data remain scarce on many glaciers. This study presents direct measurements of surface ice velocity on Grey Glacier, a major outlet glacier of the Southern Patagonian Icefield (SPI) in Chile. Ice flow was monitored over a one-week period in late 2002 by tracking the displacement of six stakes installed on the glacier surface. The resulting velocity data reveal spatial patterns of surface flow that provide significant information for the comparison and validation of remote sensing observations, which is particularly relevant considering that the ice mass from which the data were collected has since disappeared due to glacier retreat. The combined use of ground-based and remote sensing methods is essential for advancing our understanding of glacier motion and behavior, particularly in the context of climate forcing.

Keywords: glacier surface velocity; ice flow dynamics; glacier retreat; Grey Glacier; Southern Patagonian Icefield

1. Introduction

The Southern Patagonia Icefield (SPI) and the Northern Patagonia Icefield (NPI), located in Patagonia ($40\text{--}55^\circ\text{ S}$), together constitute the third-largest freshwater reserve on Earth, after Antarctica and Greenland [1–5].

These icefields have been identified as regions undergoing substantial mass loss, with frontal ablation representing a significant portion of total ablation [6–9]. Quantifying frontal ablation and understanding the dynamics of calving glaciers remain major uncertainties in projections of global glacier mass loss [8,10,11]. Surface ablation, driven by meteorological conditions, also plays a crucial role in glacier mass balance [8,12–14]. However, the lack of field observations has limited a comprehensive understanding of drivers of ablation in the SPI [13]. Studies combining remote sensing techniques with in-situ measurements are essential for improving our understanding of these processes [15,16].

While most glaciers in Patagonia are rapidly retreating, there are exceptions highlighting the complex and heterogeneous nature of glaciers response to climate change. Pio XI Glacier (49°S), the largest in Patagonia, is also one of the very few that are currently advancing [17,18]. Some glaciers have remained relatively stable or have even advanced, suggesting the influence of local factors such as precipitation patterns, glacier geometry, and subglacial conditions [18,19]. The dynamic behavior of glaciers such as Perito Moreno, which has exhibited frontal oscillations and ice-dam ruptures, underscores the need for continuous monitoring and detailed analysis [9].

The Patagonian Icefields, particularly the SPI, have undergone rapid retreat and significant glacier thinning in recent decades [7,20–22]. The SPI, located between Chile and Argentina, is the second-largest contiguous extrapolar icefield in the world [13]. Grey Glacier, along with Tyndall and Amalia glaciers, has experienced overall negative surface elevation changes [7]. Monitoring surface velocities and ice-front positions is essential to understanding individual responses of glaciers to climate change [7,15].

In this context, the study of surface ice velocity in temperate glaciers is crucial to understanding the dynamics of ice loss and the impacts of global climate change on these sensitive environments [15].

Glacier surface velocity is a key parameter for estimating ice volume variations in response to global warming and its subsequent impact on sea-level rise [15,23]. Traditional methods for measuring ice velocity fields often involve cross-correlating pairs of satellite images to track feature displacement between two acquisition dates [15]. However, direct methodologies, such as GPS measurements, offer high precision and temporal resolution, enabling detailed analysis of glacier dynamics [16]. Recent research has highlighted the heterogeneous changes occurring within the SPI, showing variability in both the magnitude and timing of individual glacier responses [9]. Understanding these variations requires detailed, site-specific studies that capture the complex interplay of climatic, topographic, and glaciological factors influencing glacier behavior [9,24].

Nevertheless, studies based on direct in situ observations that characterize ice mass movements, essential for surface mass balance and energy balance models, remain extremely limited in this region [6,8,11].

This study focuses on Grey Glacier, a major outlet glacier in the SPI, to investigate its recent dynamic behavior using direct GPS measurements of surface ice velocity [16,24]. The primary objective is to obtain empirical in situ data on glacier surface motion by measuring ice velocity from stakes installed near the glacier terminus [16].

The results provide valuable insights into the processes driving glacier change in the SPI and contribute to improving future projections of ice mass loss and sea-level rise [8,15]. This is particularly relevant given that the ice mass where the measurements were taken has gone due to the glacier's continued retreat [7,9,15].

2. Materials and Methods

To quantify short-term surface ice motion, an area of approximately 0.5 km² was selected near the frontal zone of the westernmost terminus of Grey Glacier. A set of stakes was installed roughly perpendicular to the main flow direction, aligned transversely to the central axis of the glacier tongue. This stake deployment strategy is commonly used in glaciological studies, as it allows for monitoring ice flow across a defined transect [25–28]. Each stake was vertically drilled into the ice to a stable depth and georeferenced using a GPS device [29]. The use of GPS in stake measurements enables precise tracking of stake positions over time [30,31].

After a seven-day interval, all stakes were removed, and their positions remeasured using the same GPS device. This temporal resolution is appropriate for capturing short-term variations in ice velocity [32–34]. Horizontal displacements were calculated as vector differences between initial and final stake positions in Universal Transverse Mercator (UTM) coordinates. This displacement calculation method is standard in glaciology, providing a quantitative measure of ice motion [29].

For each stake, the total displacement, average daily velocity, and direction of motion (azimuth), relative to geographic north were derived. These parameters offer a comprehensive description of ice motion at each stake location [35].

All measurements were compiled into a geospatial dataset and visualized using vector plots. These plots are commonly used to visualize glacier surface velocities and facilitate the identification of spatial patterns in ice flow [36]. The resulting displacement vectors were interpreted in the context of the local glacier geometry and expected ice flow dynamics near the terminus. This analysis enhances our understanding of the relationship between ice flow and frontal dynamics [37,38].

2.1. Study Site

This study was conducted on Grey Glacier, one of the principal outlet glaciers of the SPI (Figure 1). This glacier flows into Lago Grey, located in Torres del Paine National Park, Chile ($50^{\circ}59'S$, $73^{\circ}10'W$), through three distinct lobes at present (Figure 2). The terminus flows through a geologically complex area characterized by intense folding, which influences ice dynamics in this sector.

The study focuses on the western terminus, approximately 0.5 km from the ice front at the time of data collection (Figure 2b). Grey Glacier is a temperate, dynamic calving glacier that is highly sensitive to seasonal climatic variations [39]. Since the 1980s, the western terminus has retreated by more than 2 km, greater than the retreat observed at the other two termini, showing a trend consistent with other Patagonian glaciers [39–41].

As a result, the glacier ice, over which the data were collected, has since disappeared (Figure 2c). This fact is particularly relevant, as it enables a clearer examination of the underlying subglacial bedrock topography, which may help contextualize the findings of this study. According to water depth soundings conducted by Sugiyama et al. (2019) [42], the maximum depth near the eastern terminus is approximately 300 m (Figure 3c).

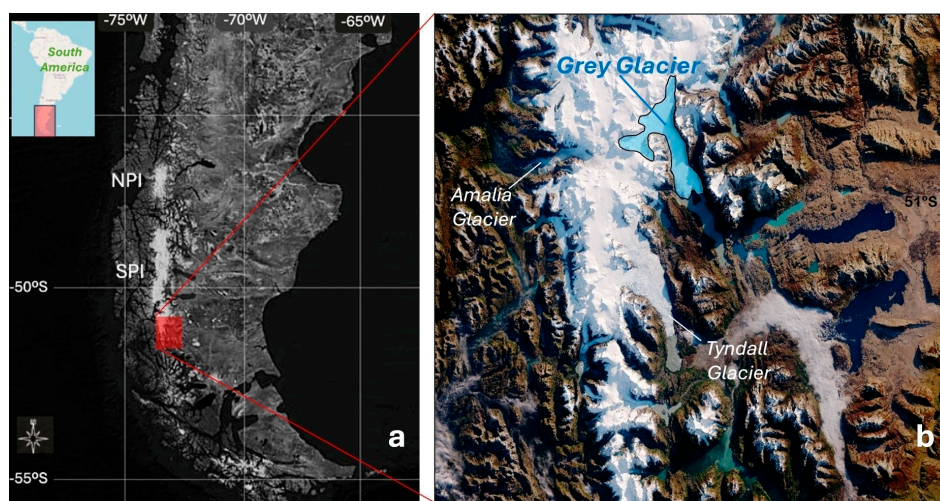


Figure 1. Geographic location of Grey Glacier. (a) Extent of the NPI and SPI in Patagonia. The inset shows the location of Patagonia in South America. (b) Location and approximate extent of Grey Glacier in the southeastern part of the SPI. The background is a false-color mosaic from a Landsat 7 ETM+ image acquired in 2001. White areas indicate regions covered by snow or ice.

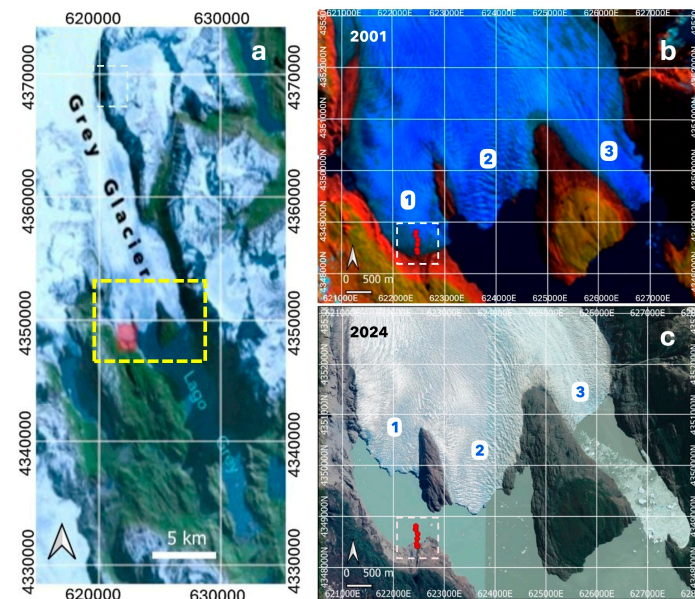


Figure 2. Location of the study area in Grey Glacier. (a) Terminus of Grey Glacier (yellow rectangle). The data collection zone is marked in red within the rectangle. (b) and (c) are enlargements of the rectangle shown in (a), showing detailed Landsat satellite views of the Grey Glacier front in 2001 and 2024, respectively. The glacier flows into Lago Grey through three distinct termini: 1, 2, and 3. Stake installation was carried out at terminus 1. The red dots within the dashed white rectangle indicate the initial stake positions and the surveyed area, approximately 0.5 km².



Figure 3. Set of photographs showing characteristics of the study area and fieldwork activities. (a) Panoramic view of the Grey Glacier front in November 2002. At that time, the glacier had a discontinuous front with three main termini (1, 2, and 3), a configuration that remains today (Figure 2c). (b) Fieldwork during the installation of stakes on the glacier surface (November 29, 2002). (c) Heavily crevassed glacier surface in the surveyed area.

2.2. Glacier Stake Installation and GPS Survey

To directly measure surface ice velocity, six iron stakes (120 cm in length, 14 mm in diameter) were manually installed vertically into the glacier surface along a transect perpendicular to the central flowline of the western lobe of Grey Glacier (Figure 3b). Installation was carried out ensuring adequate vertical alignment and sufficient insertion depth to minimize the risk of stake loss due to surface melting or toppling. The stakes were placed at intervals of approximately 50-100 m, extending toward the central flow axis, to capture local spatial variability while maintaining logistical feasibility for retrieval.

Each stake was surveyed using a Garmin eTrex handheld GPS device. Coordinates were recorded in UTM coordinate system (Easting [E], Northing [N], Zone 18F South, WGS84 datum). Under clear-sky conditions, the estimated horizontal positional accuracy was $\pm 2-5$ meters, consistent with the device's specifications.

Initial positions (E_i, N_i) were recorded on 29 November 2002, and final positions (E_f, N_f) were obtained exactly seven days later, on 6 December 2002, using the same observation procedure. During both surveys, the GPS receiver was held stationary for at least 30 seconds to enhance accuracy through signal averaging.

2.3. Displacement and Velocity Calculation

Surface ice velocity was determined from the horizontal displacement between the initial and final positions of each stake. For each stake, the displacement vector was calculated based on the

differences in the eastward (ΔE) and northward (ΔN) components in UTM coordinates between the two GPS measurements:

$$\Delta E = E_{final} - E_{initial}$$

$$\Delta N = N_{final} - N_{initial}$$

The total horizontal displacement (D) was calculated using the Euclidean distance formula:

$$\text{Displacement (D)} = \sqrt{(\Delta E)^2 + (\Delta N)^2} \quad (1)$$

Mean velocity (V) was computed as:

$$\text{Velocity (V)} = \frac{\text{Displacement (m)}}{\Delta t \text{ (day)}} \quad (2)$$

where ΔE and ΔN represent changes in easting and northing, respectively, and Δt is the time interval in days. Data storage and analysis were performed using spreadsheets in Microsoft Excel.

2.4. Flow Direction and Displacement Angle

Vector analysis of stake displacements on the glacier surface can reveal the approximate general direction of ice flow. This general flow direction is interpreted as the weighted average of the displacement vectors of all stakes.

To determine the prevailing direction of surface ice flow in the study area, we analyzed horizontal displacements and azimuthal angles (expressed in degrees clockwise from true north) of six stakes measured over a seven-day period during the summer season.

For each stake, the eastward (dx) and northward (dy) Cartesian components of displacement were calculated using the following trigonometric relationships derived from the measured displacement vectors:

$$dx = D \cdot \sin(\theta) \quad (3)$$

$$dy = D \cdot \cos(\theta) \quad (4)$$

where:

- D is the horizontal displacement (in meters),
- θ is the azimuthal direction (in degrees),
- dx and dy represent the eastward and northward Cartesian components of displacement, respectively.

The net flow vector was obtained by summing the individual eastward and northward displacement components of all stakes:

$$\begin{aligned} \sum dx \\ \sum dy \end{aligned}$$

The azimuthal direction of the resultant horizontal flow vector (θ) was calculated using the arctangent function as follows:

$$\theta = \arctan 2(\sum dx, \sum dy) \quad (5)$$

Angles were expressed in both radians and degrees to facilitate the geometric interpretation of ice motion.

2.5. Accuracy and Limitations

Given the use of a handheld GPS device, the absolute accuracy of individual stake positions is limited. However, relative displacements over short time intervals can still provide reasonable estimates of surface velocity, provided that consistent measurement conditions are maintained [43]. The expected uncertainty in horizontal displacement is estimated at ± 5 m. This level of precision is generally sufficient for resolving bulk ice motion in small- to medium-scale field studies [44].

2.6. Data Handling

All GPS data were converted and projected into UTM coordinates using QGIS v3.40 Geographic Information System (GIS) software. Displacement vectors were then visualized and analyzed to assess spatial consistency and to detect any anomalous stake movements, such as those potentially caused by melting, tilting, burial, or stake loss. Only the six glacier stakes considered potentially valid were included in this analysis. Valid vectors were visualized and cross-verified on a satellite basemap, allowing comparison with the glacier flow patterns previously identified from satellite imagery and earlier studies. For this purpose, ASTER, Landsat, and Sentinel satellite images were used, processed and visualized with tools such as USGS Earth Explorer, Copernicus Brower, Google Earth Engine and Earth Pro.

3. Results

Despite the logistical challenges inherent to fieldwork in the southernmost region of Patagonia, all planned measurements were successfully carried out. Following the recovery of the stakes after a seven-day observation period, the resulting surface displacement data were obtained as follows:

3.1. Horizontal Displacement

During a short-term field campaign conducted between 29 November and 6 December 2002, six stakes (S1 to S6) were deployed near the terminus of Grey Glacier. Each stake was installed by drilling into the glacier surface, and its initial position was recorded using a GPS receiver (UTM coordinates, Zone 18F South, WGS84 datum). After a seven-day interval, all stakes were revisited and their final positions recorded, allowing for the calculation of horizontal displacement vectors (Equation 1) and surface velocities (Table 1).

Table 1. GPS-derived horizontal displacement and surface flow direction near the terminus of Grey Glacier over a seven-day period.

Stake ID	Initial Date D/M (200 2)	Initial Easting [m] ¹	Initial Northing [m] ¹	Final Date D/M (200 2)	Final Easting [m] ¹	Final Northing [m] ¹	Displacement [m]	Azimuth (grades)
S1	29/1 1	0622469	4348417	6/12	0622478	434841 4	9,49	107,078229° E
S2	29/1 1	0622456	4348470	6/12	0622457	434846 4	6,08	169,181124° E
S3	29/1 1	0622467	4348567	6/12	0622479	434857 7	15,62	48,837797° E
S4	29/1 1	0622476	4348658	6/12	0622482	434865 5	6,71	115,208358° E
S5	29/1 1	0622437	4348748	6/12	0622460	434874 5	23,20	96,075186° E
S6	29/1 1	0622442	4348809	6/12	0622456	434880 3	15,23	111,842339° E

¹ UTM coordinates, Zone 18F South. The data were referenced to WGS84 datum.

3.1.1. Magnitude of Displacement

Measured surface displacements over a seven-day period ranged from 6.08 m (S2) to 23.20 m (S5). Stake S5, positioned closer to the central flowline, exhibited the greatest displacement, suggesting a pronounced longitudinal gradient in flow velocity near the glacier terminus.

A general trend of increasing displacement toward the south is evident, consistent with the glacier's slope and terminus morphology. This spatial pattern supports the presence of accelerated ice flow toward the calving front, a characteristic commonly observed in tidewater and lake-terminating glaciers, where basal conditions and longitudinal stress gradients play a significant role in controlling ice dynamics [39,40].

3.1.2. Stake Flow Directions

Flow directions were calculated as azimuths of the displacement vectors relative to geographic north (measured clockwise). Most vectors fall within a southeasterly quadrant (approximately 96° to 115°), consistent with the principal flow direction of Grey Glacier (Figure 1). However, significant deviations were observed at S2 (169°) and S3 (48.8°), suggesting localized variations in ice flow dynamics (Figure 4).

These directional anomalies may be associated with lateral shear zones, subglacial topographic controls, or flowline divergence and convergence near the glacier front. Such deviations highlight the complex flow regime characteristic of fast-flowing outlet glaciers.

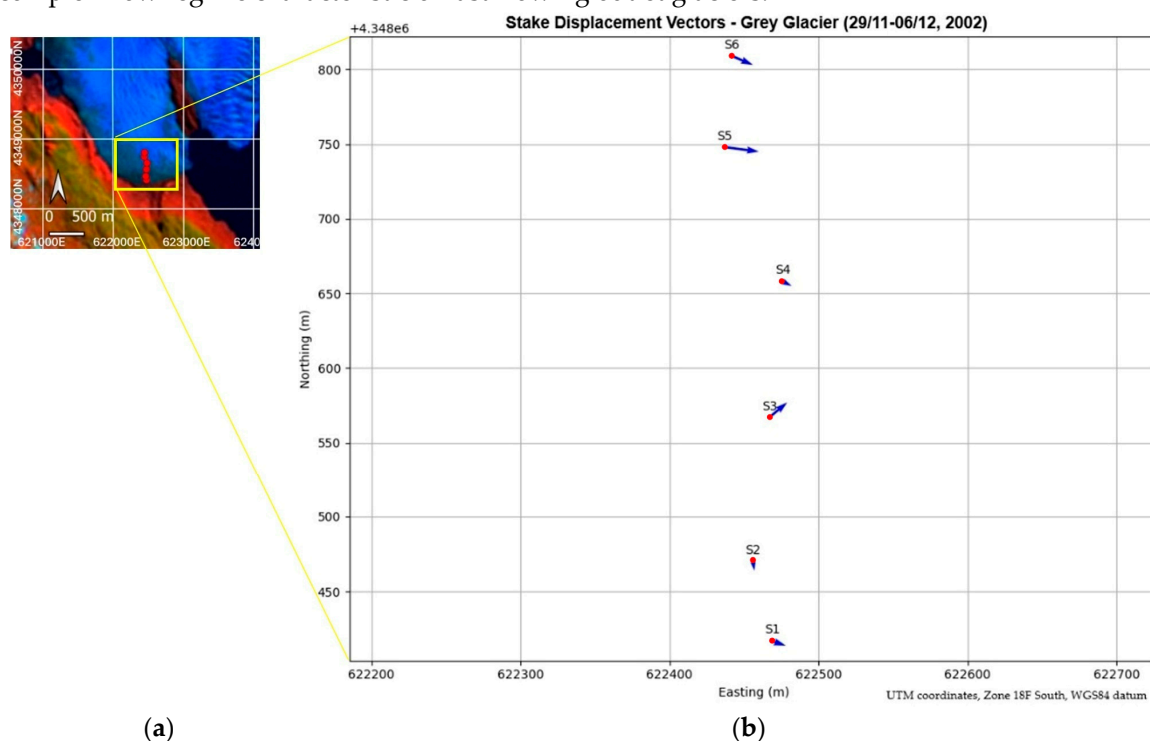


Figure 4. (a) Study area (Figure 2b). (b) Surface ice displacement vectors near the terminus of Grey Glacier, recorded between 29 November and 6 December 2002. Red points correspond to the initial positions of the stakes. Blue arrows represent the horizontal displacement of stakes (S1 to S6), based on GPS measurements in UTM coordinates. Each vector indicates both the magnitude and direction of surface ice movement over the seven-day interval. Vector length is proportional to displacement magnitude, with a reference scale provided by the UTM grid. Ice flow is predominantly oriented southeastward, consistent with glacier surface slope and overall morphology toward Lago Grey (see Figure 2a).

3.1.3. General Surface Ice Flow Direction

To estimate the overall surface ice flow direction in this sector of Grey Glacier, horizontal displacement measurements from the six stakes were analyzed. The magnitude and azimuth of each displacement vector were decomposed into Cartesian components to determine the general flow direction (Table 2).

For each stake, the eastward (dx) and northward (dy) components were calculated using trigonometric decomposition of the displacement vectors, as defined by Equations 3 and 4.

The average of the eastward and northward vector components across all six stakes was used to determine the overall direction of surface ice motion:

$$\sum dx = 65,251, \sum dy = -9,457$$

$$\sum dx = \frac{65,251}{6} \approx 10.87 \text{ m}$$

$$\sum dy = \frac{-9,457}{6} \approx -1,576 \text{ m}$$

The resultant flow vector was calculated by summing the individual eastward and northward components. Its orientation was then determined using the arctangent function (Equation 5):

$$\theta = \arctan 2 (\sum dx, \sum dy)$$

$$\theta = \arctan 2 (10.87, -1,576) \approx 98.2^\circ$$

The resultant vector indicates a general ice flow direction of approximately 98.2° , corresponding to an east-southeastward movement (Figure 5). This flow orientation reflects the deflection of the ice mass in this sector, likely influenced by the underlying topography.

Table 2 summarizes the measured horizontal displacements and the corresponding calculated vector components for each stake:

Table 2. General surface ice flow direction, eastward and northward vector components.

Stake ID	Displacement (m)	Direction (°E)	Radians	dx (m)	dy (m)
S1	9.49	107.078	1.869	9.072	-2.787
S2	6.08	169.181	2.953	1.141	-5.972
S3	15.62	48.838	0.852	11.760	10.281
S4	6.71	115.208	2.011	6.071	-2.858
S5	23.20	96.075	1.677	23.070	-2.455
S6	15.23	111.842	1.952	14.137	-5.666

Figure 5 shows the individual displacement vectors along with the resultant flow vector.

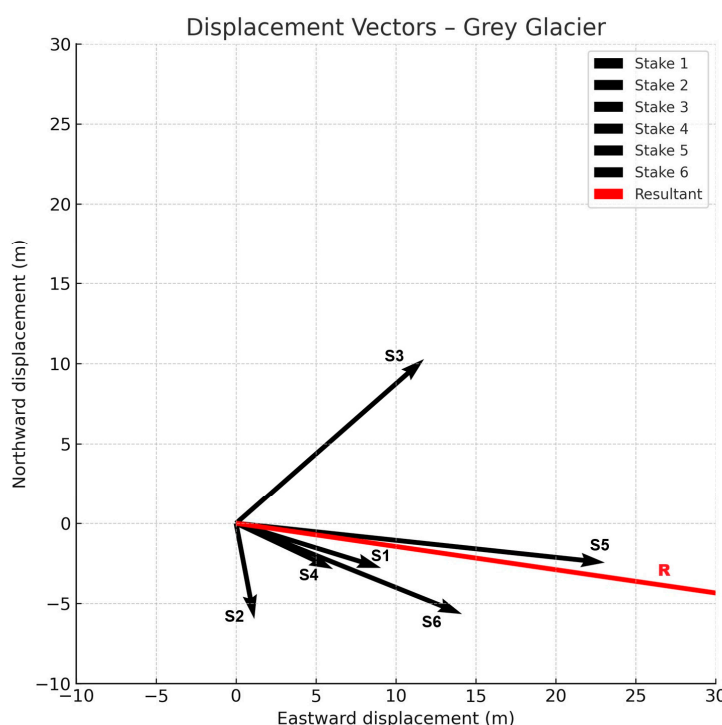


Figure 5. Individual stake displacements and resultant flow vector near the terminus of Grey Glacier. The general ice surface flow direction in the surveyed area, represented by the resultant vector (R), is approximately 98.2° from east, indicating a predominant east-southeastward motion. This vector represents the average horizontal displacement over a one-week period during the summer season and can be interpreted as the dominant strain axis at this location. Directional variability observed at stakes S2 and S3 suggests localized flow complexity, likely influenced by surface topography or basal hydrological conditions. These deviations highlight the spatial variability of ice dynamics near the glacier front and may be relevant for understanding short-term changes in frontal stress regimes.

3.2. Surface Ice Velocity

Surface ice velocity for each stake was calculated using Equation (2). The resulting velocities reveal significant spatial variability in ice flow near the terminus of the glacier across the six sampled locations. Table 3 presents the calculated surface velocities corresponding to each stake.

Table 3. Surface ice velocities measured at each stake near the terminus of Grey Glacier.

Stake ID	Displacement (m)	Time Interval (days)	Velocity (m/day)
S1	9,49	7	1,356
S2	6,08	7	0,869
S3	15,62	7	2,231
S4	6,71	7	0,959
S5	23,20	7	3,314
S6	15,23	7	2,176

Although the direct measurements of surface ice velocity show some localized anomalies, a clear transverse velocity gradient was observed: minimum velocities occurred near the glacier margins, while maximum values were recorded closer to the central flowline. This pattern is consistent with laminar flow behavior, in which lateral drag reduces ice velocity near the margins.

Measured surface velocities ranged from 0.869 to 3.314 m/day, with a mean velocity of approximately 1.817 m/day. The highest velocity was recorded at stake S5 (3.314 m/day), located near the central axis, while the lowest was observed at stake S2 (0.869 m/day), situated closer to the eastern margin. Stakes positioned near the central flowline (e.g., S5, S3, S6) exhibited higher velocities, whereas lateral stakes (e.g., S2, S4) moved more slowly.

Stakes S2 and S4, which recorded significantly lower velocities, may lie within shear margins or zones of enhanced basal friction. These conditions could be influenced by subglacial topography or spatial variability in basal water pressure [28,45]. Some rocky outcrops, revealed by the glacier's accelerated retreat since the time of data collection, provide additional support for this hypothesis.

The broader range of azimuthal directions, particularly at S2, may indicate localized flow divergence, transverse motion, or interaction with marginal pinning points. Directional data generally show eastward to east-southeastward motion, with some angular dispersion among stakes.

A weak positive relationship between elevation and velocity was noted, with slightly higher velocities at stakes located at greater elevations. This trend may reflect the influence of thicker ice or basal thermal conditions that promote basal sliding. The observed east-southeastward displacement supports convergent flow toward the terminus, potentially constrained by basal geometry, the presence of a heavily crevassed zone (Figure 3c), and lateral resistance from valley walls (Figure 3a).

4. Discussion

The observed spatial variability in surface velocity near the terminus of Grey Glacier reflects the complex dynamic regime governing this outlet glacier. The highest velocities occurred at stakes located near the presumed central flowline, consistent with predominant basal sliding attributable to

increased ice thickness and reduced lateral drag. These findings align with previous satellite- and radar-based studies that have reported enhanced ice flow along central channels [40,45–47].

Analysis of surface ice velocity, based on direct measurements from six stakes, reveals significant variations that reflect the complex glacial dynamics near the frontal zone [40,48–50]. Observed velocities ranged from 0.869 to 3.314 m/day, with a mean of approximately 1.817 m/day. These values are consistent with those reported in previous remote sensing and in situ studies on Grey Glacier and other temperate outlet glaciers in Patagonia [40,51].

Velocity differences across the stakes may result from several interacting factors. Subglacial topography plays a key role in modulating basal friction and, consequently, ice flow [28,44,52,53]. Elevation also appears influential: in general, stakes located at lower altitudes and closer to the glacier front exhibited higher velocities, possibly due to thinner ice and reduced basal resistance [54]. However, this trend is not uniform and is likely influenced by local factors such as surface slope, basal water pressure, and lateral drag.

The direction of displacement vectors also exhibited notable variability. Although the dominant flow was generally eastward to east-southeastward, significant directional deviations were recorded at certain stakes. For instance, stake S3 showed a direction of 48.8°E, while S2 indicated 169.2°E. These anomalies may reflect flow divergence, marginal shear zones, or interactions with local bedrock features and geological structures [52,53,55] (Figure 3a).

Additionally, the influence of surface debris cover must also be considered [56]. Although specific data on debris cover was not available for this study, the presence of supraglacial debris is known to impact glacier flow dynamics, which in turn affects flow velocity.

Temporal variability in ice velocity introduces another important factor. Previous studies have shown that Patagonian glaciers have undergone dynamic changes in recent decades, with episodes of acceleration and deceleration driven by climatic and hydrological conditions [47]. Consequently, the present measurements represent only a snapshot in time and may not fully capture long-term trends in glacier behavior [57].

Taken together, the surface velocity measurements on Grey Glacier highlight the complexity of ice flow near its terminus. Variations in both velocity and direction are likely governed by a combination of subglacial topography, elevation, surface debris cover, and temporal evolution [49]. These findings contribute to a better understanding of Grey Glacier's dynamic behavior and its response to external forcing such as climate change [58–60].

For future research, it is recommended to extend velocity monitoring campaigns to capture seasonal and interannual variability [61]. Detailed mapping of subglacial topography and debris cover is also needed to better constrain their influence on ice dynamics [52,62]. Ground-based measurements could be further integrated with satellite remote sensing data, including Synthetic Aperture Radar (SAR) imagery, to develop a more comprehensive picture of glacier flow [43,63–65]. In addition, numerical modeling efforts can help simulate observed patterns and predict future changes under different climate scenarios [66,67].

It is important to note that Grey Glacier, like other glaciers in Patagonia, is undergoing accelerated retreat as a consequence of climate warming [49]. Rising air temperatures have increased melt rates, contributing to mass loss and global sea-level rise [68]. Therefore, continued monitoring is essential to improve our understanding of glacier-climate interactions and inform mitigation and adaptation strategies [60–69].

5. Conclusions

This stake-based velocity survey provides new insights into the spatial variability of ice flow near the terminus of Grey Glacier. The results reveal pronounced differences in both flow velocity and direction over short distances, indicating complex interactions among basal geomorphological conditions, ice thickness, and flow geometry. These observations are essential for validating remote sensing data and improving numerical models of glacier dynamics and future ice mass changes across the SPI.

The dataset offers a valuable benchmark for ice flow modeling and supports further investigations into frontal dynamics, including calving processes and seasonal variability. It also underscores the importance of ground-based measurements in capturing small-scale variations that are often missed by remote sensing, particularly in fast-flowing outlet glaciers such as Grey Glacier.

Flow in the surveyed section is predominantly directed east-southeastward, consistent with the glacier surface morphology and the orientation of Lago Grey. However, the divergent flow directions observed at stakes S2 and S3 suggest localized structural complexity, potentially related to shear zones, flow convergence, or subglacial topographic features that deflect flow locally.

The recorded displacement vectors provide reliable point-scale data for calibrating and validating ice flow models, offering a baseline for predicting dynamic glacier responses under future climatic or geomorphological changes. The highest velocities were observed at stakes S5 and S6 (up to approximately 3.3 m/day at S5), indicating enhanced ice flow toward the south. This localized acceleration is likely driven by gravitational stress associated with surface slope, increased basal lubrication near the lake margin, and possibly to rapid block falls commonly occurring in heavily crevassed areas.

These in situ measurements highlight the dynamic nature of the glacier terminus and underscore the need for high-resolution observations to capture fine-scale variations in ice flow. The persistence of high surface velocities suggests ongoing dynamic mass loss driven by basal sliding and calving, reinforcing concerns about the glacier's stability under continued climatic forcing.

The relatively moderate velocities observed indicate stable surface motion during the measurement period (Austral summer), without indications of short-term acceleration typically associated with subglacial hydrological events. However, longer-term monitoring and repeated measurements are required to resolve potential seasonal or interannual variability in ice flow.

The results contribute to the expanding dataset of surface velocity measurements in Patagonia and support the integration of direct measurements with remote sensing techniques. A key outcome of this study is the establishment of contemporary surface velocity measurements near the glacier's terminus—a sector that has since undergone significant retreat [18,19,31,40]. These data provide a valuable reference for understanding both past and ongoing changes in the dynamic behavior of Grey Glacier in the context of regional climate change.

Funding: This research was funded by Gobierno de España / Ministerio de Educación, Cultura y Deporte (AP-2000-1152).

Acknowledgments: I thank Mr. Marco Cordero Valenzuela, Director of the Corporación Nacional Forestal de Chile (CONAF) in Punta Arenas, XII Región de Magallanes y Antártica Chilena, for his support and warm welcome, which enabled the successful execution of research in Torres del Paine National Park. I am especially grateful to the Park Administrator, Mr. Jovito González, for the facilities and assistance provided throughout the study. I also extend my sincere appreciation to the park rangers—Angelo, Jorge, Alexis, and Gorka—for their valuable support and companionship during the expeditions, and in particular, for their assistance with fieldwork on the National Park's glaciers.

Conflicts of Interest: The author declares no conflicts of interest.

Abbreviations

The following abbreviations are used in this manuscript:

SPI	Southern Patagonian Icefield
NPI	Northern Patagonian Icefield
UTM	Universal Transverse Mercator
GIS	Geographic Information System
GPS	Global Positioning System
SAR	Synthetic Aperture Radar

References

1. Warren, C.R.; Sugden, D.E. The Patagonian icefields: A glaciological review. *Arctic and Alpine Research* **1993**, *25*, 316–331. <https://doi.org/10.2307/1551915>
2. Aniya, M. Glacier Inventory for the Northern Patagonia Icefield, Chile, and Variations 1944/45 to 1985/86. *Arctic and Alpine Research* **1988**, *20*, 179–187. <https://doi.org/10.1080/00040851.1988.12002663>
3. Aniya, M.; Sato, H.; Naruse, R.; Skvarca, P.; Casassa, G. The use of satellite and airborne imagery to inventory outlet glaciers of the Southern Patagonia Icefield, South America. *Photogrammetric Engineering & Remote Sensing* **1996**, *62*, 1361–1369.
4. Rignot, E.; Rivera, A.; Casassa, G. Contribution of the Patagonia Icefields of South America to sea level rise. *Science* **2003**, *302*, 434–437. <https://doi.org/10.1126/science.1087393>
5. Rivera, A.; Casassa, G. Ice elevation, areal, and frontal changes of glaciers from National Park Torres del Paine, Southern Patagonia Icefield. *Arctic and Alpine Research* **2004**, *36*, 379–389. [https://doi.org/10.1657/1523-0430\(2004\)036\[0379:IEAAFC\]2.0.CO;2](https://doi.org/10.1657/1523-0430(2004)036[0379:IEAAFC]2.0.CO;2)
6. Aniya, M.; Sato, H.; Naruse, R.; Skvarca, P.; Casassa, G. Recent Glacier Variations in the Southern Patagonia Icefield, South America. *Arctic and Alpine Research* **1997**, *29*, 1–12. <https://doi.org/10.2307/1551831>
7. Luzardi, A.C.M.; Cárdenas, C. Recent dynamical features of Tyndall and Grey Glaciers, from Southern Patagonian Icefield, by using satellite remote sensing techniques. *International Archives of the Photogrammetry, Remote Sensing and Spatial Information Sciences* **2020**, *XLII-3/W12*, 453–458. <https://doi.org/10.5194/isprs-archives-XLII-3-W12-2020-453-2020>
8. Minowa, M.; Sakakibara, D.; Sugiyama, S.; Skvarca, P. Frontal ablation and mass loss of the Patagonian icefields. *Earth and Planetary Science Letters* **2021**, *561*, 116811. <https://doi.org/10.1016/j.epsl.2021.116811>
9. Lannutti, E.; Lenzano, M.G.; Vacaflor, P.; Rivera, A.; Moragues, S.; Gentile, M.; Lenzano, L. Ice thickness distribution and stability of three large freshwater calving glaciers on the eastern side of the Southern Patagonian Icefield. *Cold Regions Science and Technology* **2024**, *221*, 104158. <https://doi.org/10.1016/j.coldregions.2024.104158>
10. Weidemann, S.S.; Sauter, T.; Malz, P.; Jaña, R.; Arigony-Neto, J.; Casassa, G.; Schneider, C. Glacier Mass Changes of Lake-Terminating Grey and Tyndall Glaciers at the Southern Patagonia Icefield Derived From Geodetic Observations and Energy and Mass Balance Modeling. *Frontiers in Earth Science* **2018**, *6*, 81. <https://doi.org/10.3389/feart.2018.00081>
11. Dussaillant, I.; Berthier, E.; Brun, F.; Masiokas, M.M.; Hugonnet, R.; Favier, V.; Rabatel, A.; Pitte, P.; Ruiz, L. Two decades of glacier mass loss along the Andes. *Nature Geoscience* **2019**, *12*, 802–808. <https://doi.org/10.1038/s41561-019-0432-5>
12. Carrasco, J.F.; Casassa, G.; Rivera, A. Meteorological and climatological aspects of the Southern Patagonia Icefield. In *The Patagonian Icefields*; Casassa, G., Sepúlveda, F.V., Sinclair, R.M., Eds.; Springer: New York, NY, USA, 2002; pp. 29–41. https://doi.org/10.1007/978-1-4615-0645-4_4
13. Bravo, C.; Ross, A.N.; Quincey, D.J.; Cisternas, S.; Rivera, A. Surface ablation and its drivers along a west–east transect of the Southern Patagonia Icefield. *Journal of Glaciology* **2021**, *68*, 305–318. <https://doi.org/10.1017/jog.2021.92>
14. Castillo-Llarena, A.; Retamal-Ramírez, F.; Bernales, J.; Jacques-Coper, M.; Rogozhina, I. Climate and ice sheet dynamics in Patagonia during the Last Glacial Maximum. *Climate of the Past* **2023**, *19*, 1105–1126. <https://doi.org/10.5194/cp-2023-47>
15. Euillard, L.D.; Euillard, P.A.; Riveros, N.C.; Masiokas, M.H.; Ruiz, L.; Pitte, P.; Elefante, S.; Casu, F.; Balbarani, S. Detection of glaciers displacement time-series using SAR. *Remote Sensing of Environment* **2016**, *184*, 188–198. <https://doi.org/10.1016/j.rse.2016.07.003>
16. Schwalbe, E.; Krohnert, M.; Koschitzki, R.; Johnson, E.; Cárdenas, C.; Maas, H.-G. Determination of spatio-temporal velocity fields at Grey Glacier using terrestrial image sequences and optical satellite imagery. In *Proceedings of the 2017 First IEEE International Symposium of Geoscience and Remote Sensing (GRSS-CHILE)*, Valparaíso, Chile, 21–22 March 2017; pp. 1–6. <https://doi.org/10.1109/grss-chile.2017.7996022>
17. Rivera, A. Pio XI glacier: The exception to the deglaciation trend in Patagonia. *Rev. Geogr. Chile Terra Australis* **2018**, *54*, 1–12. <https://doi.org/10.23854/07199562.2018541Rivera1>
18. Piret, L.; Bertrand, S.; Moffat, C.; Feldens, P.; Papenmeier, S.; Arz, H. Recent ice-contact delta formation in front of Pio XI glacier controls sedimentary processes in Eyre Fjord, Patagonia. *Earth Surface Processes and Landforms* **2024**, *49*, 5054–5068. <https://doi.org/10.1002/esp.6012>

19. Hata, S.; Sugiyama, S. Changes in the Ice-Front Position and Surface Elevation of Glaciar Pío XI, an Advancing Calving Glacier in the Southern Patagonia Icefield, From 2000–2018. *Frontiers in Earth Science* **2021**, *8*, 576044. <https://doi.org/10.3389/feart.2020.576044>
20. Davies, B.; Darvill, C.; Glasser, N.; Hein, A.; Martin, J.; Smedley, R.; Smellie, J.; Thorndycraft, V.; Geiger, A.; Harrison, S.; et al. The Patagonian Ice Sheet from the last glacial cycle to the Present Day. In *EGU General Assembly Conference Abstracts*; European Geosciences Union: Munich, Germany, 2018; Volume 20, p. 4605.
21. Huynh, C.; Hein, A.S.; McCulloch, R.D.; Bingham, R.G. The last glacial cycle in southernmost Patagonia: A review. *Quaternary Science Reviews* **2024**, *344*, 108972. <https://doi.org/10.1016/j.quascirev.2024.108972>
22. García, J.-L.; Hall, B.L.; Kaplan, M.R.; Gómez, G.A.; De Pol-Holz, R.; García, V.J.; Schaefer, J.M.; Schwartz, R. ¹⁴C and ¹⁰Be dated Late Holocene fluctuations of Patagonian glaciers in Torres del Paine (Chile, 51°S) and connections to Antarctic climate change. *Quaternary Science Reviews* **2020**, *246*, 106541. <https://doi.org/10.1016/j.quascirev.2020.106541>
23. Jiskoot, H.; DeJong, E.; Van Wychen, W.; Cooley, J. The need for global glacier speed to combine measured velocity with balance velocity. *EGU General Assembly Conference Abstracts 2020*, *EGUsphere*, EGU2020-12515. <https://doi.org/10.5194/egusphere-egu2020-12515>
24. Vries, M.; Wickert, A. Glacier Image Velocimetry: An open-source toolbox for easy and rapid calculation of high-resolution glacier-velocity fields. *The Cryosphere* **2021**, *15*, 2115–2132. <https://doi.org/10.5194/tc-15-2115-2021>
25. Chadwell, C.D. Reliability analysis for design of stake networks to measure glacier surface velocity. *Journal of Glaciology* **1999**, *45*, 154–164. <https://doi.org/10.3189/S0022143000003130>
26. Fountain, A.G.; Vecchia, A.V. How many stakes are required to measure glacier velocity? *Geografiska Annaler: Series A, Physical Geography* **1999**, *81*, 563–573. <https://doi.org/10.1111/1468-0459.00084>
27. Cogley, J.G.; Adams, W.P.; Ecclestone, M.A.; Jung-Rothenhäusler, F.; Ommann, C.S.L. Mass balance of White Glacier, Axel Heiberg Island, N.W.T., Canada, 1960–91. *Journal of Glaciology* **1996**, *42*, 548–563. <https://doi.org/10.3189/s0022143000003531>
28. Sugiyama, S.; Fukui, K.; Fujita, K.; Tone, K.; Yamaguchi, S. Changes in ice thickness and flow velocity of Yala Glacier, Langtang Himal, Nepal, from 1982 to 2009. *Annals of Glaciology* **2013**, *54*, 157–162. <https://doi.org/10.3189/2013aog64a111>
29. Sugiyama, S.; Bauder, A.; Riesen, P.; Funk, M. Surface ice motion deviating toward the margins during speed-up events at Gornergletscher, Switzerland. *Journal of Geophysical Research: Earth Surface* **2010**, *115*, F03025. <https://doi.org/10.1029/2009jf001509>
30. Telling, J.; Glennie, C.; Fountain, A.; Finnegan, D. Analyzing Glacier Surface Motion Using LiDAR Data. *Remote Sensing* **2017**, *9*, 283. <https://doi.org/10.3390/rs9030283>
31. Jansson, P. Longitudinal coupling in ice flow across a subglacial ridge. *Annals of Glaciology* **1997**, *24*, 169–174. <https://doi.org/10.3189/s026030550001212x>
32. Hubbard, B. Direct measurement of basal motion at a hard-bedded, temperate glacier: Glacier de Tsanfleuron, Switzerland. *Journal of Glaciology* **2002**, *48*, 1–8. <https://doi.org/10.3189/172756502781831610>
33. Liu, L.; Jing, Z.F.; Zhang, X.J. The application of GPS in glacier flow velocity: A case study of Qiyi Glacier. *Applied Mechanics and Materials* **2011**, *130–134*, 1794–1798. <https://doi.org/10.4028/www.scientific.net/AMM.130-134.1794>
34. Chadwell, C.D.; Hardy, D.R.; Braun, C.; Brecher, H.H.; Thompson, L.G. Thinning of the Quelccaya Ice Cap over the last thirty years. *The Cryosphere Discuss* **2016**, *tc-2016-40*. <https://doi.org/10.5194/tc-2016-40>
35. Bartholomaus, T.C.; Anderson, R.S.; Anderson, S.P. Response of glacier basal motion to transient water storage. *Nature Geoscience* **2008**, *1*, 33–37. <https://doi.org/10.1038/ngeo.2007.52>
36. Jacobel, R.W. Short-Term Variations in Velocity of South Cascade Glacier, Washington, U.S.A. *Journal of Glaciology* **1982**, *28*, 325–332. <https://doi.org/10.3189/s0022143000011667>
37. Singh Jasrotia, A.; Ahmad, S.; Ridwan, Q.; Ahmad Wani, Z.; Siddiqui, S.; Siddiqua, A.; Ali Morfeine aika, E. Estimation of Surface Ice Velocity of Durung Drung Glacier, Western Himalaya using COSI-Corr from Landsat images. *The Egyptian Journal of Remote Sensing and Space Sciences* **2024**, *27*, 369–381. <https://doi.org/10.1016/j.ejrs.2024.04.006>
38. Bhattacharjee, S.; Garg, R.D.; Pandey, A.C. Monitoring glacier surface velocity in Zanskar Valley, India: Insights from DInSAR-based 2D velocity estimation. *Results in Earth Sciences* **2025**, *3*, 100092. <https://doi.org/10.1016/j.rines.2025.100092>

39. Rivera, A.; Bown, F.; Castillo, A.; Oberreuter, J.; Lenzano, M.G.; Lenzano, L. Southern Patagonia Icefield freshwater calving glaciers recent collapses into deep lake waters. In *Proceedings of the EGU General Assembly 2021*; EGU: Vienna, Austria, 2021. <https://doi.org/10.5194/egusphere-egu21-10265>

40. Sakakibara, D.; Sugiyama, S. Ice-front variations and speed changes of calving glaciers in the Southern Patagonia Icefield from 1984 to 2011. *J. Geophys. Res. Earth Surf.* **2014**, *119*, 2541–2554. <https://doi.org/10.1002/2014jf003148>

41. Yamamoto, Y. Recent frontal variations and driving mechanisms of Glaciar Grey in the Southern Patagonia Icefield. Master's Thesis, Hokkaido University, Sapporo, Japan, 2018.

42. Sugiyama, S.; Minowa, M.; Schaefer, M. Underwater ice terrace observed at the front of Glaciar Grey, a freshwater calving glacier in Patagonia. *Geophysical Research Letters* **2019**, *46*, 1361–1369. <https://doi.org/10.1029/2018GL081441>

43. Heid, T.; Kääb, A. Evaluation of existing image matching methods for deriving glacier surface displacements globally from optical satellite imagery. *Remote Sensing of Environment* **2012**, *118*, 339–355. <https://doi.org/10.1016/j.rse.2011.11.024>

44. Cuffey, K.M.; Paterson, W.S.B. *The Physics of Glaciers*, 4th ed.; Academic Press: Amsterdam, The Netherlands, 2010.

45. Rignot, E.; Rivera, A.; Casassa, G. Contribution of the Patagonia Icefields of South America to sea level rise. *Science* **2003**, *302*, 434–437. <https://doi.org/10.1126/science.1087393>

46. Rivera, A.; Benham, T.; Casassa, G.; Bamber, J.; Dowdeswell, J.A. Ice elevation and areal changes of glaciers from the Northern Patagonia Icefield, Chile. *Global and Planetary Change* **2007**, *59*, 126–137. <https://doi.org/10.1016/j.gloplacha.2006.11.037>

47. Muto, M.; Furuya, M. Surface velocities and ice-front positions of eight major glaciers in the Southern Patagonian Ice Field, South America, from 2002 to 2011. *Remote Sensing of Environment* **2013**, *139*, 50–59. <https://doi.org/10.1016/j.rse.2013.07.034>

48. Naruse, R.; Aniya, M.; Skvarca, P.; Casassa, G. Recent variations of calving glaciers in Patagonia, South America, revealed by ground surveys, satellite-data analyses and numerical experiments. *Annals of Glaciology* **1995**, *21*, 297–303. <https://doi.org/10.3189/S0260305500015974>

49. Stocker-Waldhuber, M.; Fischer, A.; Helffricht, K.; Kuhn, M. Ice flow velocity as a sensitive indicator of glacier state. *The Cryosphere Discuss.* **2018**, *tc-2018-37*. <https://doi.org/10.5194/tc-2018-37>

50. Willis, M.J.; Melkonian, A.K.; Pritchard, M.E.; Rivera, A. Ice loss from the Southern Patagonian Ice Field, South America, between 2000 and 2012. *Geophysical Research Letters* **2012**, *39*, L17501. <https://doi.org/10.1029/2012GL053136>

51. Kamb, B.; Echelmeyer, K.A. Stress-gradient coupling in glacier flow: I. Longitudinal averaging of the influence of ice thickness and surface slope. *Journal of Glaciology* **1986**, *32*, 267–284. <https://doi.org/10.3189/S0022143000015604>

52. Paterson, W.S.B. *The Physics of Glaciers*, 3rd ed.; Pergamon Press: Oxford, UK, 1994.

53. Mouginot, J.; Rignot, E. Ice motion of the Patagonian Icefields of South America: 1984–2014. *Geophysical Research Letters* **2015**, *42*, 1441–1449. <https://doi.org/10.1002/2014gl062661>

54. Mertes, J.R.; Thompson, S.S.; Booth, A.D.; Gulley, J.D.; Benn, D.I. A conceptual model of supra-glacial lake formation on debris-covered glaciers based on GPR facies analysis. *Earth Surface Processes and Landforms* **2016**, *42*, 903–914. <https://doi.org/10.1002/esp.4068>

55. Echelmeyer, K.; Zhongxiang, W. Direct observation of basal sliding and deformation of basal drift at sub-freezing temperatures. *Journal of Glaciology* **1987**, *33*, 83–98. <https://doi.org/10.3189/S002214300005396>

56. Da Huo; Bishop, M.P.; Young, B.W.; Chi, Z.; Haritashya, U.K. Numerical modeling issues for understanding complex debris-covered glaciers. In *Treatise on Geomorphology*, 2nd ed.; Shroder, J.F., Ed.; Academic Press: Cambridge, MA, USA, 2022; Volume 4.08, pp. 143–168. <https://doi.org/10.1016/B978-0-12-818234-5.00019-5>

57. Wen, M.; Wang, T. Review of SAR imaging geodesy for glacier velocity monitoring. *Geodesy and Geodynamics* **2025**, *16*, 262–274. <https://doi.org/10.1016/j.geog.2024.08.004>

58. Post, A.; O'Neil, S.; Motyka, R.J.; Streveler, G. A complex relationship between calving glaciers and climate. *Eos, Transactions American Geophysical Union* **2011**, *92*, 305–306. <https://doi.org/10.1029/2011EO370001>

59. Azam, M.F.; Wagnon, P.; Berthier, E.; Vincent, C.; Fujita, K.; Kargel, J.S. Review of the status and mass changes of Himalayan–Karakoram glaciers. *Journal of Glaciology* **2018**, *64*, 61–74. <https://doi.org/10.1017/jog.2017.86>

60. Jiskoot, H.; DeJong, E.; Van Wychen, W.; Cooley, J. The need for global glacier speed to combine measured velocity with balance velocity. *EGU General Assembly 2020, EGUSphere*, egu2020-12515. <https://doi.org/10.5194/egusphere-egu2020-12515>
61. Yuan, X.; Qiao, G.; Li, Y. 57-year ice velocity dynamics in Byrd Glacier based on multisource remote sensing data. *IEEE Journal of Selected Topics in Applied Earth Observations and Remote Sensing 2023, PP*, 1–24. <https://doi.org/10.1109/JSTARS.2023.3250759>
62. Zorzut, V.; Ruiz, L.; Rivera, A.; Pitte, P.; Villalba, R.; Medrzycka, D. Slope estimation influences on ice thickness inversion models: A case study for Monte Tronador glaciers, North Patagonian Andes. *Journal of Glaciology 2020*, 66, 996–1005. <https://doi.org/10.1017/jog.2020.64>
63. Frezzotti, M.; Capra, A.; Vittuari, L. Comparison between glacier ice velocities inferred from GPS and sequential satellite images. *Annals of Glaciology 1998*, 27, 54–60. <https://doi.org/10.3189/1998AoG27-1-54-60>
64. Gao, J.; Liu, Y. Applications of remote sensing, GIS and GPS in glaciology: A review. *Progress in Physical Geography 2001*, 25, 520–540. <https://doi.org/10.1177/030913330102500404>
65. Ahn, Y.; Howat, I.M. Efficient automated glacier surface ice speed measurement from repeat images using multi-image/multichip and null exclusion feature tracking. *IEEE Transactions on Geoscience and Remote Sensing 2011*, 49, 2838–2846. <https://doi.org/10.1109/TGRS.2011.2114891>
66. Carturan, L.; Cazorzi, F.; Dalla Fontana, G.; Zanoner, T. Automatic measurement of glacier ice ablation using thermistor strings. *Journal of Glaciology 2019*, 65, 219–227. <https://doi.org/10.1017/jog.2018.103>
67. Fahrner, D.; Catania, G.; Shahin, M.G.; Hansen, D.D.; Löffler, K.; Abermann, J. Advances in monitoring glaciological processes in Kalallit Nunaat (Greenland) over the past decades. *PLOS Climate 2024*, 3, e0000379. <https://doi.org/10.1371/journal.pclm.0000379>
68. Carrivick, J.L.; Tweed, F.S.; Sutherland, J.L.; Mallalieu, J. Toward numerical modeling of interactions between ice-marginal proglacial lakes and glaciers. *Front. Earth Sci. 2020*, 8, 577068. <https://doi.org/10.3389/feart.2020.577068>
69. Caro, A.; Condom, T.; Rabatel, A. Climatic and morphometric explanatory variables of glacier changes in the Andes (8–55° S): New insights from machine learning approaches. *Front. Earth Sci. 2021*, 9, 713011. <https://doi.org/10.3389/feart.2021.713011>

Disclaimer/Publisher's Note: The statements, opinions and data contained in all publications are solely those of the individual author(s) and contributor(s) and not of MDPI and/or the editor(s). MDPI and/or the editor(s) disclaim responsibility for any injury to people or property resulting from any ideas, methods, instructions or products referred to in the content.